Supplemental Data

Building Complexity: An In Vitro Study of Cytoplasmic Dynein with In Vivo Implications

Roop Mallik, Dmitri Petrov, S.A. Lex, S.J. King, and S.P. Gross

Supplemental Section 1: Characterization of Bead Flop

The linkage between the motor domain of dynein and the cargo is flexible, which allows the bead to flop around the position of the motor while the motor is attached to a fixed position on the microtubule. Due to noise arising from such thermally induced flop, there are large instantaneous velocities in the position-versus-time data, which have no obvious connection to the mechanochemical properties of the motor. It is therefore important to estimate and exclude the effects of this floppy motion.

To do this, we first incubated beads with dynein in the absence of ATP and then flowed them through a coverslip with immobilized microtubules. After beads underwent a period of incubation in the coverslip, we could observe them bound to microtubules under the microscope. These beads were not motile, but they displayed thermally induced flop (both along and perpendicular to microtubules). We also characterized the flop of immotile dynein bound beads in the presence of ADP and AMP-PNP (a non-hydrolyzable form of ATP), with no ATP added. We did not detect any significant difference in the characteristics of bead flop for all three cases (no nucleotide at all, only ADP, and only AMP-PNP).

We used different dynein:bead ratios to find the flop properties of a tether consisting of single or multiple dyneins. As expected, we observed a general trend toward a decrease in flop for multiple motors. In Figure S1A, we show a scatterplot of position in the X-Y (X along MT; Y perpendicular to MT) plane for a flopping bead (gray circles) presumably bound to a microtubule (MT) through a single-dynein motor. A bead diffusing along the microtubule in the presence of ATP (black circles) is also shown. Note the clear difference in motion between diffusive and flopping beads. The scatterplot of a representative flopping bead (this behavior is typical of all flopping beads observed) shows that it can move out farther perpendicular to the MT than along the MT. This could be for two reasons:

1. Geometry: The MT prevents the bead from going all the way down to the coverslip in the X direction (along the MT). Perpendicular to the MT (Y), the bead could go down all the way to the coverslip.
2. The stiffness of the dynein tether could be different in the X and Y directions. This is expected because it has two binding points (the two heads) along the MT where it makes contact. So, there is additional rigidity to the structure along the MT.

A normalized histogram of displacement along the microtubule for flopping beads is shown in Figure S1B. The mean position (set to zero) is assumed to be the fixed dynein tether position on the microtubule. A Gaussian fit (thick black line) gives a standard deviation in position (σ = 36.9 nm). From this, we calculated that the flopping bead has a 0.7% chance of moving away more than ±100 nm from the tether point as a result of thermal flop. In contrast, the diffusing bead travels back and forth over several hundreds of nanometers. Also note that the spread perpendicular to the MT is the same for both flopping and diffusing beads. This shows that the diffusing bead is bound to the MT all the time, although it can diffuse back and forth along the MT.

Supplemental Section 2: Estimation of Backward Motion under Load

In Figure 1C, inset (main text), we have reported the percentage of backward motion under load for single-dynein, kinesin-1, and multiple-dynein motors. In this estimation, it is important to distinguish thermally driven random flop of the bead from backward slippage under load. This thermal flop is reduced for an optically trapped bead. Because the force due to the trap grows linearly as a function of bead distance, the motor linkage stiffness should increase in a linear fashion as the bead moves out of the trap. To estimate the magnitude of flop of a dynein bound bead in the optical trap between 50%–100% load, we looked at the standard deviation in the position of dynein-driven beads (σ_{pos}) that stalled at somewhat lower forces (between 0.5 to 0.8 pN). The value of σ_{pos} within visibly flat-stalled regions was found to be 7.1 ± 0.6 nm (n = 20). Although this is a rough estimation, this value of σ_{pos} is an overestimate of the actual value because of the possibility of steps within the visibily flat regions.

To score an event as a backward slide, we required the bead to move backward by more than 10 nm. From an autocorrelation analysis of the positions of dynein bound trapped beads, we found a correlation time of approximately 50 ms. To ensure that a scored event was actually backward slippage and not bead flop, we required that the >10 nm portion of backward slide should persist for at least 200 ms (at least four independent bead positions >10 nm). A one-tailed t test gives $p < 5\%$ probability of finding four such independent points beyond 10 nm just by random chance.

Supplemental Section 3: Estimation and Exclusion of Possible Artifacts Arising from In Vitro Conditions

Irregular motor behavior such as that observed for dynein could also arise because of the nature of in vitro experiments. For example, motor-protein function could be compromised in the artificial surroundings of a buffer-containing microscope sample chamber. Our earlier report [S1] and current observation that the in vitro dynein stall force is the same as that predicted from in vivo force measurements [S2] suggest that the motor is functioning well and is undergoing its normal mechanochemical cycle under our in vitro conditions. However, because a major conclusion of this paper is that single-dynein motors show poor motion, we present below further analysis and experiments to exclude the possibility that this poor performance of dynein is an in vitro artifact.

Transient sticking of beads to the microscope coverslip is a problem typical of in vitro experiments and could in general lead to poor qualities of motor-driven motion (e.g., lower velocities). To estimate the extent of such sticking in our assays, we parsed the video tracks of motor-driven beads into segments of constant velocity (see the Experimental Procedures in the main text). We expect that the bead would flop less when stuck, and therefore the variance in position of the bead perpendicular to the MT ($Var_{\perp}$) within a constant-velocity segment can be used as an indicator of sticking. The ability to parse data into segments allowed us to exclude segments where we suspect the bead was stuck. After parsing, we rejected all segments for which $Var_{\perp}$ was less than a threshold value (as determined from beads nonspecifically stuck to the coverslip).

Why use the perpendicular-variance instead of a velocity threshold? The perpendicular variance is a direct measure of the flop of a bead. If a bead is stuck, both the parallel (along-MT) and perpendicular variance will be low. The perpendicular variance is independent of the bead's motor-driven motion (which is along the MT) and is therefore the correct parameter to estimate bead sticking. We did not use a velocity threshold because single-dynein-driven motion shows a large inherent variation in velocity, and we did not want to exclude paused or low-velocity states. There are periods when the cargo is paused (low velocity) because of the function of the motor and not because of sticking. Our analysis allows distinction between bead sticking (low velocity and reduced perpendicular variance) and paused motor function (low velocity, but still large perpendicular variance).

The percentage of data excluded (as a fraction of total time of motion) in this manner was approximately equal for single-dynein- (7.3%) and kinesin (7.9%)-driven motion. This shows that any difference in properties of motion between these two motors reported here is not due to bead sticking.

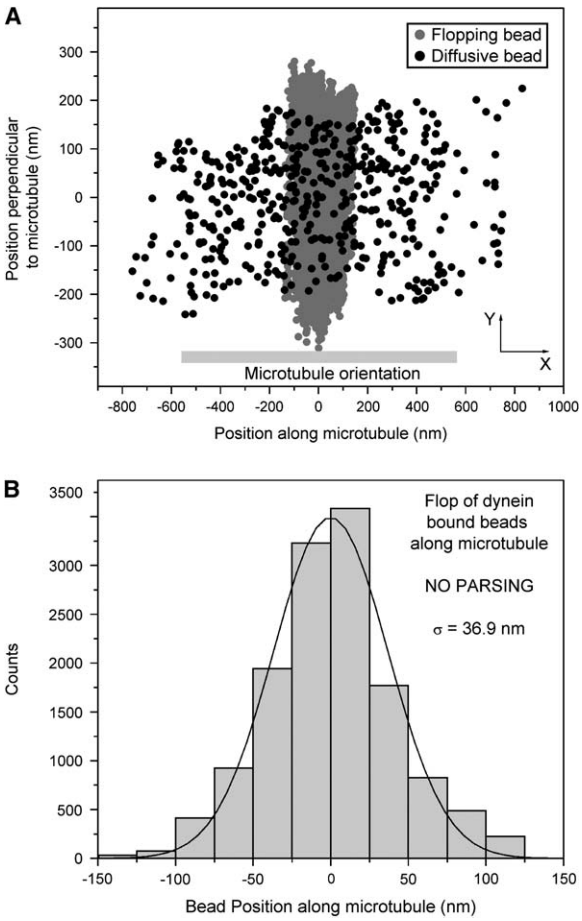

Figure S1. Characterization of Flop of Dynein Bound Beads

(A) Flop and diffusion of dynein bound beads. A scatterplot in the X-Y plane (X along MT, Y perpendicular to MT) is shown for an immotile bead tethered to the MT through a single-dynein motor in the absence of ATP (gray dots). A scatterplot for a bead diffusing along the MT (black dots) is also shown for the sake of comparison.

(B) Spread in position along the microtubule for a dynein bound flopping bead in the absence of ATP. The mean position (zero) is assumed to be the tether point. The thick black line is a Gaussian fit to the histogram and yields a standard deviation of 36.9 nm.

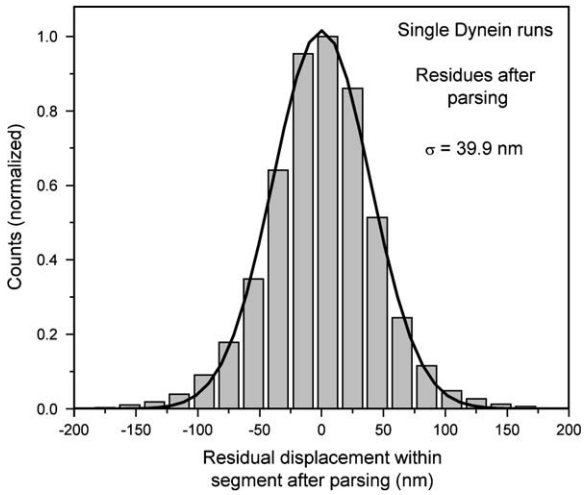

Figure S2. Residual after Multiple Single-Dynein Tracks Were Fit to Constant-Velocity Segments with the Parsing Program

The black line is a Gaussian fit yielding a standard deviation of 39.9 nm. This value is in close agreement with the spread in positions of a flopping bead bound by a single dynein (see Figure S1B).

In assays for motion in vitro, motors are usually adsorbed nonspecifically onto a bead, and it is possible that a motor does not reside in its normal in vivo-like orientation on the bead surface. To rule out the possibility that our results are compromised by abnormal bead-motor attachment/orientation, we characterized the properties of dynein function when the dynein was bound to the bead through a specific antibody-mediated attachment by using carbodiimide chemistry. We converted carboxyl groups on the bead surface [S3] into amine-reactive esters by using 1-ethyl-3-[3-dimethylaminopropyl]carbodiimide hydrochloride (EDC, Pierce, IL) as a zero-length crosslinker in the presence of Sulfo-NHS (Pierce, IL). Beads were incubated overnight in MES buffer (pH 5) with Sulfo-NHS, EDC, and rabbit polyclonal dynein light chain (H-60) IgG (Santa Cruz Biotechnology). Under these conditions, the amine-activated groups form a stable amide bond with the antibody. Activated carboxyl groups not bound to antibody were quenched with glycine to prevent further dynein binding at such sites. Such beads were then used for in vitro motility assays with dynein as described above. As a control, we prepared glycine-quenched beads in the absence of antibody, incubated them with dynein as usual, and then scored the probability that these beads would attach to MTs. At a dynein concentration where antibody-coated beads showed a 90% chance (30 tested) of binding and moving on MTs, not even a single control bead (30 tested) bound to the MT. This shows that dynein was specifically attached to the beads through the light-chain antibody in our experiments.

A dynein light-chain (LC) antibody was chosen because the LC is known to mediate cargo binding [S4, S5] at the base of the dynein molecule. Immuno-EM has clearly shown that the LCs are located at the base of the dynein molecule, at the far end from the ATP-hydrolyzing heads [S6]. Furthermore, all of the LCs are bound to the intermediate chains and not the light intermediate chains or heavy chains [S4, S7]. Therefore, the LCs are far away from the heavy chains (motor domains) of dynein, and binding dynein through a LC antibody ensures that the dynein cargo binding domain attaches to the bead, so both motor heads are free to generate force on the MT. The stall force (see Figure S5) and velocity of the light-chain antibody-attached dynein was identical (within experimental error; 26 beads tested) to that seen for nonspecifically adsorbed dynein. This shows that, under our experimental conditions, the method of nonspecific attachment does not compromise dynein function on the bead surface.

Supplemental Section 4: Parsing Program and Its Testing

The goal of our parsing procedure is to interpret molecular motor-driven bead motion as a series of states of constant velocity. Tracking data (video tracking at 30 frames/s) is presented to the parsing routine as a time series of X and Y coordinates of the cargo on a plane. The microtubule is modeled as a straight line that best fits the X-Y positions of the cargo. After finding a suitable model for the microtubule, we find the projections of the positions of the cargo on the microtubule. These projections can be interpreted as the positions (length versus time) of the motor on the microtubule. We determine constant-velocity states by fitting the length versus time data by a set of connected line segments. For this, we determine the number of segments and find the optimal positions of the ends of the segments (vertices). The task of selecting the optimal number of segments is nontrivial because in general, models with a larger number of segments will better fit the data. The program finds the minimum number of segments that describe the data to within some externally provided tolerance levels. We determine this tolerance from the flop of an immotile dynein-tethered bead.

To optimize the performance of the program, we adjusted the program parameters until the residual noise after fitting closely agreed with the distribution of positions of a dynein bound flopping bead (shown in Figure S1B). Note that the result in Figure S1B is just the observed positions of a flopping bead around a mean position from its video track. There is no use of the parsing routine in this determination. Figure S2 shows the distribution of residuals after the

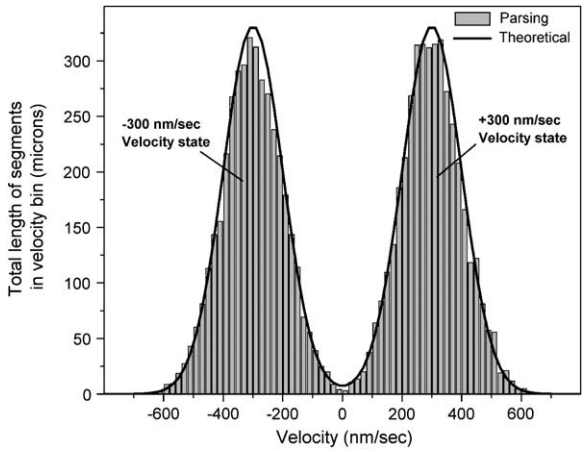

Figure S3. Test for the Parsing Routine

Artificial data (with added noise) consisting of two velocity states (+300 nm/s and −300 nm/s), and a distribution of velocity-segment lengths within each state was generated. The program is able to correctly identify all segments within a given velocity bin (see text for details).

parsing program runs on video tracks of dynein motion. The distribution of residuals is Gaussian and shows good agreement with the distribution of a flopping bead (Figure S1B). This implies that parsing is able to approximate the bead motion reliably in terms of linear constant-velocity segments. The residual left within each segment after parsing is just the flop of the bead within this segment. As mentioned earlier, this is precisely the aim of our parsing program.

To test how reliably the parsing program estimates velocities, we generated artificial video tracks with two velocity states. These states had a mean velocity of +300 nm/s and –300 nm/s and a Gaussian distribution of velocity (σ =100 nm/s) around both these mean values. The constant-velocity segments within each state had an exponentially decaying distribution of lengths, with an average length of 500 nm. Noise with characteristics similar to the thermal fluctuations of a flopping bead (see Figure S1B) was added to these tracks.

A plot of total length traveled versus velocity is shown in Figure S3. To generate this plot, we first parsed the simulated tracks into constant-velocity segments. Then we added the length of all segments lying within a velocity bin and repeated the procedure across the whole velocity range. The results from parsing (gray vertical bars) are superimposed with the known distribution (thick black line). The close agreement is evidence that the parsing routine can reliably extract all the segments pertaining to a particular velocity bin. The total distance (L) within each velocity state is the sum of all segment lengths within this state. For the –300 nm/s velocity state, L_{known}= 4153 μm and $L_{parsing}$= 4107 μm. For the +300 nm/s velocity state, L_{known}= 4153 μm and $L_{parsing}$= 4034 μm. Thus, the parsing routine is able to reliably identify velocity segments in simulated data having noise similar to the flop of dynein bound beads. Further testing and

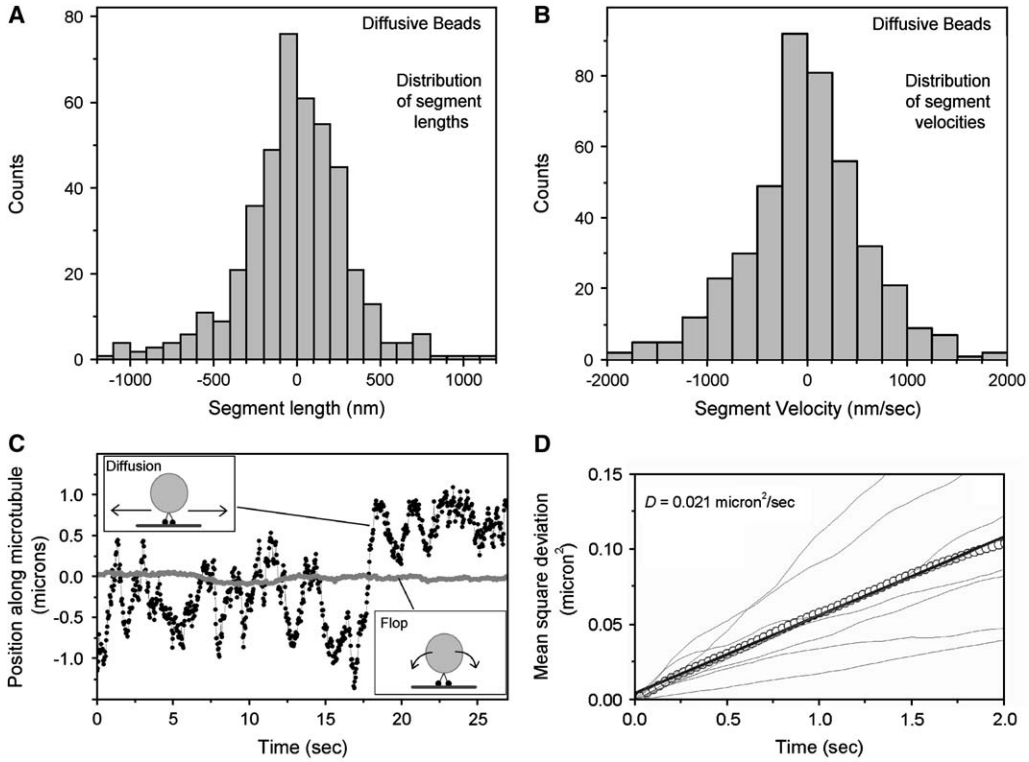

Figure S4. Properties of Diffusive Motion of Beads bound to the MT through a Dynein Tether

(A) The parsing routine was used to parse diffusive motion from video tracks (15 different beads used) into constant-velocity segments. Parameters of the program were the same as those used to determine properties of directed motion due to dynein. The accessible range of velocities is shown.

(B) The accessible range of segment lengths during diffusive motion is shown.

(C) A long segment of diffusive motion of a bead (dark circles) is shown superimposed with a flopping dynein bound bead in the absence of ATP (gray circles). The diffusing bead samples almost 2 μm of the microtubule length.

(D) The mean squared deviation of positions from seven diffusing beads as a function of time (thin gray lines) is shown. The averaged mean square deviation of these beads (hollow circles) shows a linear dependence (thick dark line) characteristic of diffusion. The linear fit yields a diffusion coefficient (D) of 0.021 μm ^{2}/s if we use $\langle x^2 \rangle = 2Dt$.

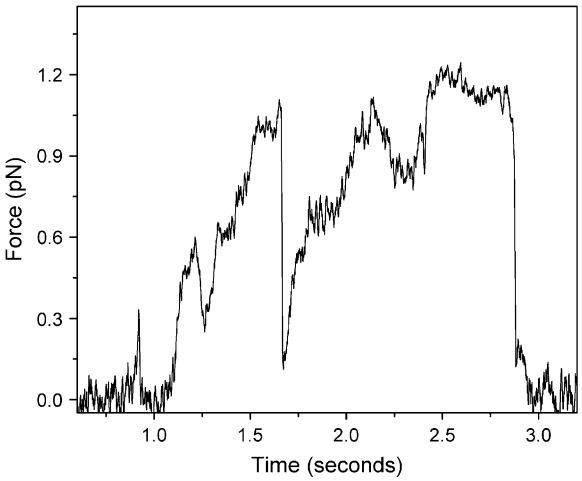

Figure S5. Representative Stall-Force Record of Single-Dynein Motor Specifically Bound to a Bead through a Dynein Light-Chain Antibody via Carbodiimide Chemistry

This attachment ensures that the cargo binding domain of dynein is attached to the bead and that both motor domains (heavy chains) are free to generate force against the microtubule. The observed stall force is the same (approximately 1 pN) as that determined from dynein attached nonspecifically to the bead (passive attachment) and also as that predicted from in vivo dynein stall-force measurements (see main text). This provides evidence that dynein is able to undergo its normal mechanochemical cycle and force generation when it is attached nonspecifically.

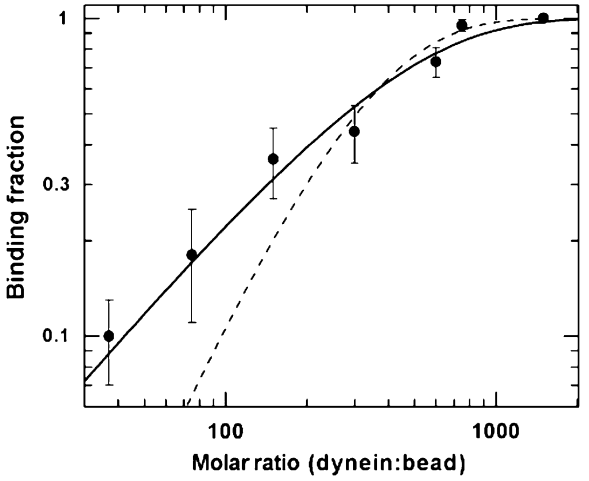

Figure S6. Bead-to-Microtubule Binding Probability as a Function of the Molar Ratio of Dynein-Coated Beads

ATP concentration = 1 mM. Solid curve is a fit to single-molecule Poisson distribution $P(n) = 1 - \exp(-n/b)$. Binding efficiency (b) from fit = 400 ± 38. Dashed curve: attempted fit to a two-molecule Poisson distribution $P(n) = 1 - \exp(-n/b) - (n/b)\exp(-n/b)$. Error bar = $\pm\sqrt{[P(1 - P)/N]}$, where P is the binding probability and N is the number of beads tested. An optical trap was used to bring dynein-coated beads into contact with immobilized MTs.

details of the algorithm will be presented elsewhere (our unpublished data).

Supplemental Section 5: Estimation of the Number of Active Motors on a Bead

Experiments to probe single-motor behavior were performed at low motor concentration, where the probability of more than one functional motor attaching to and moving a bead (also called binding fraction) is negligible [S8]. To arrive at this limit, we mapped out the fraction of beads binding as a function of motor concentration. We scored whether a motor-coated bead bound to a microtubule when the optical trap was used to place the bead in close proximity to the microtubule and confirmed that the form of the curve was consistent with the requirement of only a single motor to move the bead (see Figure S6). Single-motor assays were then performed at a bead:microtubule binding fraction of 0.5 or less. In this limit, the probability of two motors simultaneously driving the motion of a bead is <5% by Poisson statistics. Thus, in the single-motor assays, >95% of moving beads are driven by single-dynein molecules. This is confirmed by the fact that a similar force-generation profile is seen for >95% of beads moving in the optical trap.

For experiments on beads driven by two or more dyneins, we gradually increased the dynein concentration in the incubation mixture. In a concentration regime where the binding fraction was between 0.5 and approximately 0.8, we found a mixture of single- and two-dynein-driven motion with rare instances of motion driven by more than two dyneins (as estimated from stall-force measurement). There was a distinct crossover behavior in the properties of motion in this regime. Although many beads moved short distances (<1 μm, as expected for single motors) and detached, we also found beads moving over a long distance (>4 μm) before reaching the microtubule end or detaching. The motion of these long-moving beads was visibly more robust and faster than the single-dynein-driven short motion. Data reported to be two-dynein-driven motion was mostly taken from this crossover regime of dynein concentration. When the motor concentration increased further, all beads bound and moved on microtubules (binding fraction = 1). We found no short runs typical of single dyneins at this concentration. Stall-force measurements in this limit showed that approximately 60% of the beads would exert a force close to 2 pN. The rest of the beads would either stall with forces between 2 and 3.7 pN or escape from the trap. Beads escaping from the trap were estimated to exert at least a force of approximately 4 pN, in consideration of the weak nonlinear regime of trap stiffness beyond 160 nm from the center of the trap (see Figure 3C, main text).

Supplemental Section 6: Model for the Unproductive State Showing Back-and-Forth Motion of Dynein

As stated in the main text (see section "Nature of the Unproductive State"), two models could be imagined: (1) These periods reflect the motor's having a second off-pathway state where it is unproductive and which under some circumstances allows backward motion or (2) the motor has a fixed probability (P_B) of taking a backward step at every pass through its hydrolytic cycle. Differentiating between these two models is important because it has implications for understanding dynein function at the single-molecule level as well as for understanding how dynein's in vivo function is achieved. In what follows, we provide several lines of evidence to rule out the second model.

For the second model, we can estimate values of P_B that would be required to produce the characteristics of motion identified by our parsing program (see Figures 2A and 2B and Table 1 in the main text). We simulated a Poisson stepper with constant probability P_B of a back step at every step and a step size of 24 nm, which is close to the expected mean step size for dynein motion under no load [S1]. The overall net velocity reflecting the combined forward and backward motion was 200 nm/s, which is close to the velocity of single-dynein motion (Table 1). Thermal fluctuations of the position of the cargo around the motor are modeled as a confined random walk with an effective diffusion coefficient derived from video tracks of immotile flopping beads. We analyzed the simulated motion with the parsing program. For the parsing routine to detect 19% net backward motion (as seen for single dyneins; Figure 2A of the main text), we require P_B to be approximately 46% in the simulations. This is hard to imagine because it would make dynein remarkably inefficient. To further investigate the likelihood of this, we looked at the motion of dynein under load. For kinesin (and presumably dynein), when under load, the probability of back steps increases exponentially [S9]. Thus, we would expect that for dynein

under load, P_B should be >46%, which is much higher than the typical backward motion under load for single dynein (for example, see Figure 1C of the main text).

Another observation inconsistent with the second model is that dynein-driven beads never generate stalls in the plus-end direction in the optical trap. In the trap, we never observed any instance of long plus-end motion. This implies that although large excursions in the plus-end direction are possible under no load (see Figure 6 of the main text and also Figure S4C), they do not result from the motor actively generating force in the plus direction. In contrast, if the backward motion reflected diffusion (see below), force production would not be expected. Thus, from several lines of evidence, the backward segments during multiple-motor-driven motion cannot arise from motors stepping backward randomly and independently during their cycle. We therefore favor the first model, where the reverse motion arises from the motor having a second off-pathway state, which we term the "unproductive state" of dynein.

Supplemental Section 7: Properties of Diffusive Motion

We checked whether dynein-tethered beads diffusing along microtubules could give rise to the observed distribution of backward (plus-directed; see Figure 2A of the main text) motion seen for single-dynein motors. For this, we used the parsing program to find constant-velocity segments within long, diffusive segments of motion. We selected from our data pool 15 beads that had long back-and-forth periods of motion.

The parsing program had exactly the same parameters as those used in the analysis of single-dynein-driven directed motion (main text Figures 1A, 2A and 2B). The histograms of segment length and velocity are symmetric, as expected for 1D-diffusion (Figures S4A and S4B). The range of velocities and segment lengths is very similar to that of the backward (plus) motion for single-dynein motors (compare Figures S4A and S4B with Figures 2A and 2B of the main text). This shows that the segment velocities and segment lengths seen for backward motion of single dyneins are accessible through diffusive motion. Figure S4C shows a representative video track of a long segment of diffusion. The bead samples almost 2 μm of the microtubule length. To further test if such segments of motion were diffusive, we show the mean squared deviation (MSD) as a function of time of seven diffusing beads (thin gray lines). A large variation can be seen, as also observed by other workers [S10]. The average MSD as a function of time (open circles) is fitted to a straight line, yielding a diffusion coefficient of 0.021 $\mu m^2/s$, comparable to earlier reported values [S10]. The linear dependence suggests a diffusive nature of motion.

Supplemental References

S1. Mallik, R., Carter, B.C., Lex, S.A., King, S.J., and Gross, S.P. (2004). Cytoplasmic dynein functions as a gear in response to load. Nature *427*, 649–652.

S2. Gross, S.P., Welte, M.A., Block, S.M., and Wieschaus, E.F. (2000). Dynein-mediated cargo transport in vivo. A switch controls travel distance. J. Cell Biol. *148*, 945–956.

S3. Grabarek, Z., and Gergely, J. (1990). Zero-length crosslinking procedure with the use of active esters. Anal. Biochem. *185*, 131–135.

S4. King, S.J., Bonilla, M., Rodgers, M.E., and Schroer, T.A. (2002). Subunit organization in cytoplasmic dynein subcomplexes. Protein Sci. *11*, 1239–1250.

S5. Vallee, R.B., Williams, J.C., Varma, D., and Barnhart, L.E. (2004). Dynein: An ancient motor protein involved in multiple modes of transport. J. Neurobiol. *58*, 189–200.

S6. King, S.M., and Witman, G.B. (1990). Localization of an intermediate chain of outer arm dynein by immunoelectron microscopy. J. Biol. Chem. *265*, 19807–19811.

S7. King, S.M., Barbarese, E., Dillman, J.F., 3rd, Benashski, S.E., Do, K.T., Patel-King, R.S., and Pfister, K.K. (1998). Cytoplasmic dynein contains a family of differentially expressed light chains. Biochemistry *37*, 15033–15041.

S8. Svoboda, K., and Block, S.M. (1994). Force and velocity measured for single kinesin molecules. Cell *77*, 773–784.

S9. Carter, N.J., and Cross, R.A. (2005). Mechanics of the kinesin step. Nature *435*, 308–312.

S10. Wang, Z., and Sheetz, M.P. (1999). One-dimensional diffusion on microtubules of particles coated with cytoplasmic dynein and immunoglobulins. Cell Struct. Funct. *24*, 373–383.